Ann. Geophys., 31, 2137–2146, 2013
www.ann-geophys.net/31/2137/2013/
doi:10.5194/angeo-31-2137-2013


Annales Geophysicae
Open Access

# Statistical analysis of radar observed F region irregularities from three longitudinal sectors

**R. Y. C. Cueva**[1,2], **E. R. de Paula**[1], **and A. E. Kherani**[1]

[1]Aeronomy Division, DAE, National Institute for Space Research (INPE), São José dos Campos, 12227-010, São Paulo, Brazil
[2]Centro de Radio Astronomia e Astrofísica Mackenzie, CRAAM, Presbyterian Mackenzie University, São Paulo, Brazil

*Correspondence to:* R. Y. C. Cueva (rica_yvan@dae.inpe.br, ricardo.cueva@craam.mackenzie.br)

Received: 4 December 2012 – Revised: 17 October 2013 – Accepted: 30 October 2013 – Published: 3 December 2013

**Abstract.** Equatorial Spread F (ESF) is a manifestation of ionospheric interchange instabilities in the nighttime equatorial F region. These instabilities generate plasma density irregularities with scale sizes ranging from centimetres to thousands of kilometres. The irregularities can be detected from a variety of instruments such as digisonde, coherent and incoherent scatter radars, in situ space probes, and airglow photometers. In the present study, occurrence statistics of the ESF, based on various parameters are presented using data obtained from the VHF radars located at three longitudinally separated equatorial stations: Christmas Island (2° N, 202.6° E, 2.9° N dip latitude), São Luís (2.59° S, 315.8° E, 0.5° S dip latitude) and Jicamarca (12° S, 283.1° E, 0.6° N dip latitude). The ESF parameters presented here are the onset altitude, onset time (onset refers to first appearance of signal in the radar field of view) of the bottom-type and plume, and the peak altitude of the plume. Recent studies have used these parameters to classify the spread F occurrence characteristics. The present study reveals novel features namely, the dependence of ESF parameters on the seasonal, solar flux, declination angle and longitudinal dependence from the three radar sites. In addition, we also present an empirical model to determine the nature of these ESF parameters as a function of the solar flux which may enable us to forecast (with 30 min to 1 h tolerance) the plume occurrence at any longitude located in between São Luís and Christmas Island.

**Keywords.** Ionosphere (Equatorial ionosphere; Ionospheric irregularities) – Radio Science (Ionospheric physics)

## 1 Introduction

Upward developing plumes from upwelling of the bottomside F layer associated with equatorial spread F (ESF) events have been studied with VHF/UHF/L-band backscatter radars located near the geomagnetic equator (e.g. Woodman and La Hoz, 1976; Tsunoda et al., 1979; Tsunoda 1980a, b; Hysell and Burcham, 1998; de Paula et al., 2004; Kudeki et al., 2007). ESF is formed by the Rayleigh–Taylor instability in the bottomside F layer above the geomagnetic equator and it grows nonlinearly to the topside (e.g. Ossakow, 1981). Related to initiation of ESF, the eastward electric field in the dayside equatorial ionosphere is sharply intensified just before it reverses to the nightside westward direction. This intensification gives origin to the so-called evening prereversal enhancement (e.g. Rishbeth, 1971; Farley et al., 1986; Haerendel et al., 1992; Abdu, 2005) which is responsible for the initiation of the Rayleigh-Taylor instability by increasing both the gravitational and electrodynamic terms of the growth rate (e.g. Fejer et al., 1999; Abdu, 2001). It has been established that the height of the post-sunset F layer is the most important parameter controlling the generation of equatorial spread F (e.g. Farley et al., 1970; Abdu et al., 1983; Jayachandran et al., 1993; Fejer et al., 1999).

Much of the advances in studying the equatorial spread-F phenomena resulted from VHF backscatter radar measurements (e.g. Farley et al., 1970; Woodman and La Hoz, 1976; Kudeki et al., 2007; Rodrigues et al., 2004). The ESF phenomenon occurrence covers a wide spectrum of scale sizes ranging from few centimetres to hundreds of kilometres, and varies with longitude, local time, season and solar and geomagnetic activity. The irregularities can be

detected by coherent and incoherent scatter radars, in situ space probes, radio propagation, and airglow detectors in addition to ionosondes. Although the irregularities represent a continuum of scales, most remote techniques for observing them are sensitive to particular scale sizes (Basu et al., 1978).

A series of papers had discussed the occurrence patterns of bottom-type, bottomside, and topside echoes (e.g. Hysell and Farley, 1996; Hysell and Burcham, 1998, 2002; Hysell, 2000). Bottom-type and bottomside spread F layers are both scattering layers that exist in the bottom side of the F region. Bottomside layers frequently appear subsequent to bottom-type layers, the reverse does not happen. Bottom-type layers are narrowed and confined to a small range of altitudes under the action of a still westward zonal electric field. They do not present much vertical development. This layer cause very less spreading in the ionograms. The bottomside layer is considerably more intense and structured broad scattering layer than the bottom-type layer and occasionally give rise to small plumes penetration into the topside. Bottomside layers are those that emerge in regions of the ionosphere controlled by the F region dynamo (Hysell and Farley, 1996; Hysell and Burcham, 1998). These layers drift eastward. Radar plumes are evidence of deep plasma depletion rising up through the F peak under the influence of well-developed instabilities and entering to the topside. Large-scale radar plumes seem to occur frequently in the time interval of transition from bottom-type to bottomside layers, where the F region flow changes from westward to eastward.

Determining the behaviour of F region plasma irregularities in the nighttime equatorial ionosphere as a function of longitude is vital for understanding the physics of their development/occurrence. We focus on spread F occurrence statistics based on longitude, solar flux-dependence and seasonal variations for three longitudinal sectors. This paper is organised as follows: Sect. 2 describes the instrumentation used to obtain the datasets for this work. Section 3 describes the methodology used in this study including an introduction of the spread F parameters that are obtained from radar data. In Sect. 4, we present the results and corresponding discussions and in Sect. 5, we summarise the present work.

## 2 Instrumentation and data base

In this work, we analyse the data obtained from the three coherent scatter VHF radar located at São Luís (SLZ), Christmas Island (CXI) and Jicamarca (ROJ). The geographic and geomagnetic coordinates of these equatorial stations are presented at Table 1, and their geographic positions are shown in stars over the geomagnetic field lines (Bz) map (see Fig. 1). Figure 1 represents the variation of the magnetic declination angle at each equatorial station. The declination is represented as the angle between the perpendicular line to the geomagnetic equator (blue line) and the true north (black line).

**Table 1.** Geographic and geomagnetic coordinates of the equatorial ionospheric stations.

| Station | Geog. Lat. | Geog. Long. | Declination | Dip. Lat. |
|---|---|---|---|---|
| SLZ | 2.59° S | 44.2° W | 20.44° W | 0.5° S |
| ROJ | 12.0° S | 76.9° W | 0.30° W | 0.6° N |
| CXI | 2.0° N | 157.4° W | 8.55° E | 2.9° N |

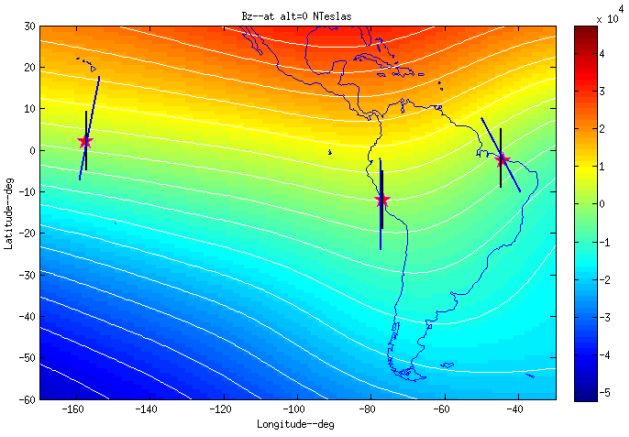


**Fig. 1.** The geographic position of the three equatorial stations are plotted in stars over the geomagnetic field lines (Bz). The field lines are plotted as Lat-Long-Bz. Modified code of magnetic field lines from Copyright© 2010, Charles Rino.

VHF radar specifications for the three equatorial stations are shown in Table 2. Details of operational and experimental issues for São Luís radar can be found in de Paula and Hysell (2004), de Paula et al. (2004) and Rodrigues et al. (2004, 2008); in Woodman and Hagfors (1969); Kudeki and Bhattacharyya (1999), for Jicamarca radar; and Tsunoda et al. (1995); Miller et al. (2009, 2010) and Makela et al. (2009), for Christmas Island radar.

## 3 Methodology

Coherent scatter radar observations of the ionospheric plasma irregularities are usually displayed in range time intensity (RTI) format, in which the backscatter power is plotted against altitude and time. Figure 2 depicts an ESF event at SLZ radar on 1 December 2002. The figure shows the backscatter signal-to-noise ratio in dB versus altitude (in km) and time (in UT). The colour bar shows $(S-N)/N$ index from $-5$ to 20 dB units. Intense backscatter indicates the presence of strong plasma irregularities with 5 m scale size. Indicated in black lines and labels are the spread F parameters used. This image is a classic representation of spread F observed over São Luís station during high spread F activity.

**Table 2.** VHF Radar specifications for the three equatorial stations in use. For Jicamarca some details are separated for 2003–2006 and 2007–2013 period.

| | São Luís | Jicamarca (2003–2006/2007–2013) | Christmas Island |
|---|---|---|---|
| Frequency | 30 MHz | 50 MHz | 50 MHz |
| Peak Power | 4 kW | 1.5 MW | 16 kW |
| Antenna half-power-full-beam-width | 10° | 1° | 2.3° |
| Inter-pulse-period (IPP) | 9.34 ms (1400 km) | 13.33 ms (2000 km)/6.25 ms (937.5 km) | 2.6 ms (782 km) |
| Altitude coverage | 87.5–1267.5 km | 79.95–1961.85 km/0–926.25 km | 83.9–865.96 km |
| Velocity coverage | $\pm 250\,\mathrm{m\,s^{-1}}$ | $\pm 112\,\mathrm{m\,s^{-1}}/\pm 240\,\mathrm{m\,s^{-1}}$ | $\pm 250\,\mathrm{m\,s^{-1}}$ |
| Altitude resolution | 2.5 km (6.6 micros) | 2.55 km (6.7 micros)/3.75 km (9.86 micros) | 8.75 km (23.02 micros) |
| Noise Band Width | 120 KHz | 120 KHz | 100 KHz |
| Small-scale irregularities in view | 5 m | 3 m | 3 m |

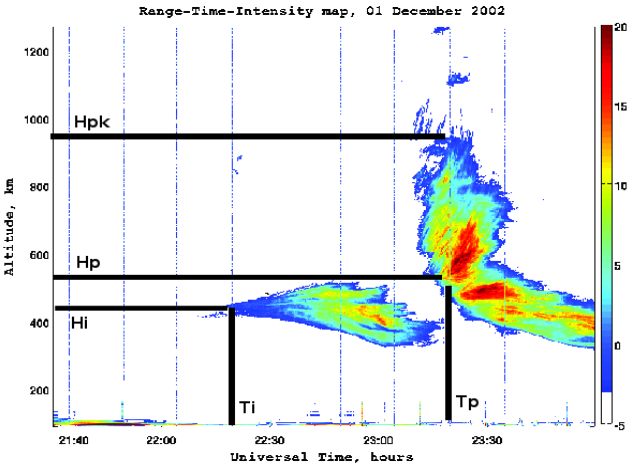


**Fig. 2.** Plume characteristics observed at São Luís station on 1 December 2002. The VHF radar parameters are highlighted in black labels, where $T_\mathrm{i}$ and $T_\mathrm{p}$ parameters mean the onset time of the bottom-type and the plume, respectively. The $H_\mathrm{i}$, $H_\mathrm{p}$ and $H_\mathrm{pk}$ parameters mean the onset altitude of the bottom-type, onset altitude of the plume and peak altitude of the plume, respectively.

The present study is based on identifying spread F parameters that are suggested by recent studies (Fejer et al., 1999; Hysell and Burcham, 2002; Chapagain et al., 2009; de Paula et al., 2011). Based on the morphological features, these studies have classified the irregular structures as bottom-type/bottomside layers and topside plume. These parameters are $T_\mathrm{i}$ and $H_\mathrm{i}$ representing the time and altitude of the first appearance of bottom-type and bottomside layers, $T_\mathrm{p}$, $H_\mathrm{p}$, and $H_\mathrm{pk}$ representing the time and altitude of the first appearance of the plume, and the peak altitude of the plume respectively. The identification of parameters are based on RTI map where $(S-N)/N$ is plotted. $(S-N)/N$ greater than $-10$ dB is considered for the estimations of these parameters. Therefore, these ESF parameters may change since the aforementioned criteria depend on the highly varying noise level with season and solar flux.

In this work, the radar data from SLZ during 2001–2008, from CXI during 2003–2009 and from ROJ during 2001–2009 are used. The datasets from SLZ and ROJ cover the solar-maximum to solar-minimum periods, and the dataset from CXI covers the descending solar-maximum to the extended solar-minimum period. In order to examine the seasonal behaviour, we grouped the data in three seasons: equinox (March–April and September–October) and December/June solstices (November to February/May to August) irrespective of the solar flux. For SLZ/ROJ, December/June solstices are respectively summer and winter solstices and for CXI, which is located in the Northern Hemisphere. For SLZ/ROJ, winter solstice data are not presented owing to the lack of observations.

## 4 Results and discussion

### 4.1 Seasonal and longitudinal occurrences of spread F parameters over CXI and comparison with São Luís and Jicamarca

In this section, we present the seasonal and longitudinal occurrences of ESF observed by the three equatorial VHF radars. In Table 3, the observation and occurrence statistics of ESF are presented, based on the seasons. The occurrence statistics is further classified into two groups: ESF with bottom-type and ESF with plume. It should be noted that the ESF with plume may occur with and without bottom-type ESF. Figure 3 depicts the occurrence statistics of ESF where total days of occurrence of ESF (shown as white histogram) and the total days of ESF with plume (shown as black histogram) are plotted for each month.

From CXI, we note the following characteristics: (1) the % occurrence of ESF is maximum during summer solstice month of August and secondary maximum is in equinoctial September month, (2) the % occurrence is minimum during winter-solstice month of February and equinoctial March–April, (3) the % occurrence of the plume also follows the seasonal trend of % occurrence of ESF, (4) the % occurrence

**Table 3.** Spread F occurrence over Christmas Island, São Luís and Jicamarca stations, separated by radar signatures.

| | Equinox | Nov–Feb | May–Aug | Signatures |
|---|---|---|---|---|
| CXI | 527 | 473 | 644 | Observations |
| | 61 (11.58 %) | 55 (11.63 %) | 74 (11.49 %) | Bottom-type |
| | 160 (30.36 %) | 122 (25.70 %) | 236 (36.65 %) | Plume |
| SLZ | 259 | 265 | 65 | Observations |
| | 105 (40.54 %) | 37 (13.96 %) | 10 (15.38 %) | Bottom-type |
| | 139 (53.67 %) | 216 (81.51 %) | 0 (0 %) | Plume |
| ROJ | 362 | 438 | 390 | Observations |
| | 90 (24.86 %) | 154 (35.16 %) | 51 (13.08 %) | Bottom-type |
| | 168 (46.41 %) | 182 (41.55 %) | 64 (16.41 %) | Plume |

of bottom-type ESF is similar during all seasons. Comparisons among CXI/SLZ/ROJ reveal the following characteristics: (5) the season of maximum % occurrence of ESF is summer-solstice (May–August for CXI and November–February for SLZ/ROJ) for all three stations, (6) % of occurrence of ESF during these maximum occurrence seasons is greater (smaller) than 50 % over CXI (SLZ/ROJ), (7) the season of maximum % occurrence of ESF with plume is summer-solstice for CXI/SLZ and is equinox for ROJ, (8) % of occurrence of plume during these maximum occurrence seasons is $\sim$ 80 % over SLZ, $\sim$ 50 % over ROJ and $\sim$ 36 % over CXI, (9) % of occurrence of plume during the minimum occurrence seasons is $\sim$ 0 % over SLZ, $\sim$ 16 % over ROJ and $\sim$ 25 % over CXI, (10) % occurrence of the bottom-type ESF shows seasonal dependence over SLZ/ROJ compared to the no seasonal dependence over CXI.

The characteristics noted under (1–3) are known from the previous study by Makela et al. (2004). Characteristics noted under (4–10) bring additional aspects in the present study. It is evident that the total % occurrence of ESF and plume during season of maximum occurrence is lowest over CXI and highest over SLZ. Similarly, % occurrence of bottom-type ESF is also minimum over CXI and maximum over SLZ. These aspects suggest that the Ionospheric-Atmospheric conditions over SLZ (CXI) are most (least) favourable for the generation of ESF, among three stations. ROJ has % occurrence characteristics more similar towards SLZ except that the season of maximum occurrence of ESF with plume is during equinox, which is a known feature from earlier studies (Basu et al., 1980; Sobral et al., 2002; de Paula et al., 2011). However, it is interesting to note that the season of maximum occurrence of all ESF events (i.e. with and without plume) is summer-solstice for all three stations. Thus, as far as the generation of ESF is concerned, the summer-solstice season offers most favourable conditions.

We may point out that, for CXI, the dataset mainly covers the descending solar-maximum to entire solar-minimum period. Therefore, the results for CXI are mainly corresponds to the solar minimum. For this reason, the maximum ESF occurrence is found to be during summer-solstice in the present study, which is known from the previous studies.

The seasonal difference in the maximum occurrence of ESF plume and the seasonal indifference in the maximum occurrence of all ESF over three stations brings an important aspect for consideration: the seasonal difference in maximum occurrence over SLZ and ROJ is owing to the finite magnetic declination angle effect as explained by de Paula et al. (2011) based on the mechanism suggested by Abdu et al. (1981). Abdu et al. (1981) found that the seasonal dependence of sunset vertical drift and spread F (and scintillation) occurrence at a given longitude are controlled by the magnetic declination angle, and high occurrence is expected during the months when the conjugate E layers enter darkness at the same time with a consequent integrated Pedersen conductivity decrease. Owing to the finite declination angle over SLZ (20° W), a required alignment is achieved during summer-solstice, leading to the maximum occurrence of ESF with plume event during this season. On the other hand, over Jicamarca with almost zero declination (declination angle being $\sim$ 0.5° W), the alignment is achieved during equinox leading to the maximum occurrence of ESF with plume event during this season. The declination effects in the occurrence of ESF with plume between SLZ and ROJ is reported by previous studies. However, with the inclusion of CXI, the present study shows that the similar declination effects are present over CXI which has finite declination angle ($\sim$ 8.55° E), achieving the required alignment during summer-solstice, thus leading to the maximum occurrence of ESF with plume event during summer-solstice, similar to SLZ. Moreover, it is noted that the total ESF occurrence is maximum during summer-solstice over all three stations. It indicates that is the occurrence of ESF with plume, and not the total ESF occurrence, that is controlled by the declination angle.

The seasonal behaviour of the bottom-type ESF, as noted under (10) is another noteworthy aspect to discuss. The seasonal behaviour of the bottom-type ESF over SLZ in the present study reveals similar characteristics as recently reported by de Paula et al. (2011) and is explained on the basis of the collisional-interchange instability mechanism that leads to the formation of a sharp bottomside structure (instead of the plume) owing to the strong velocity shear and low gravity wave seeding amplitude. The season of maximum occurrence of the bottom-type ESF over ROJ is summer-solstice while occurrence remains unaltered with season over CXI. Thus, the bottom-type ESF reveal varying degree of the occurrence characteristics with longitude.

### 4.2 Solar-flux dependence during season of maximum occurrence of ESF with plume

In order to examine the solar-flux dependence of the ESF occurrence, we select the season of maximum occurrence of ESF with plume, i.e. summer-solstice for CXI/SLZ and

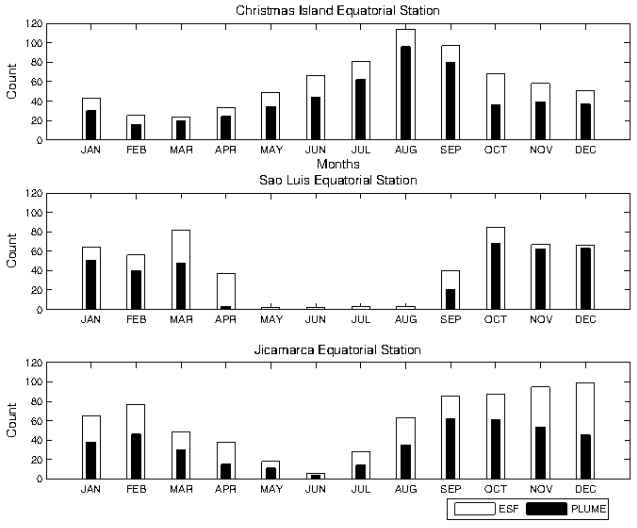


**Fig. 3.** Seasonal occurrence of spread F irregularities combined for over the period in study (irrespective of solar flux). In white bars are the spread F events, and in black bars the plume events observed over each equatorial station.

equinox for ROJ. In Fig. 4a–c, we depict the solar-flux dependence in the following format: in the upper panel from left-to-right columns, the ESF parameters ($H_i$, $H_p$), ($T_i$, $T_p$) and ($H_p$, $H_{pk}$) are plotted respectively. These values represent the 4 month average values and corresponding standard deviations are plotted as the error bars. In the middle-lower panels, the data-points that are used to estimate the average values in the corresponding upper panel, are shown. We note that with increasing solar-flux, ($H_i$, $H_p$ and $H_{pk}$) increase and ($T_i$, $T_p$) decrease. These characteristics are known for SLZ and ROJ from the previous studies. The present study suggests that over CXI, the ESF parameters have similar solar-flux dependency. We then note that, for a given solar-flux value, the onset time of ESF and plume are 2–3 h later over CXI as compared to the SLZ/ROJ. In particular, $T_p$ is in 22:00–23:00 LT i.e. most of the plume events over CXI are pre-midnight. We also note that both $T_i$ and $T_p$ decrease with the increasing solar-flux, but their difference $\Delta T = T_i - T_p$ increases with the increasing solar-flux over CXI. On the other hand, over ROJ, the tendency is opposite, i.e. the difference decreases. Over SLZ, the difference has tendency of slight increase with increasing solar-flux. Thus, over CXI/SLZ, the difference $\Delta T$ increases with increasing solar-flux while over ROJ, it decreases with increasing solar-flux. It suggests that with increasing solar-flux, the bottom-type/bottomside of ESF appear earlier but the plume appearance gets delayed by as much as 3 h over CXI. We also note that the height difference $\Delta H = H_p - H_{pk}$, which is representative of vertical size of plume, decreases with increasing solar-flux over CXI while it increases over SLZ and remain almost constant over ROJ. Thus, it may be said that with increasing solar-flux, the plume appearance get delayed and its vertical extent become shorter over CXI. These both characteristics suggest that over CXI, the plume occurrence is more favourable during low-solar-flux. Usually, a contrary is expected, as observed over SLZ/ROJ, i.e increasing high-solar-flux provide more favourable conditions for the occurrences of the plumes mainly owing to the equatorial dynamics such as the large prereversal vertical drift, large bottom-side density gradient and efficient seeding of gravity wave arising from the troposphere convection. Therefore, over CXI, other effects, that possibly include off-equatorial dynamics such as parallel conductivity and meridional winds, are playing important role to determine the final fate of the plume.

It should be further noted that, with increasing solar-flux, the $H_{pk}$ increases drastically over SLZ as compared to over ROJ, and remains almost constant over CXI. In other words, the bubble evolution finds more favourable equatorial and off-equatorial conditions over SLZ than other two stations. It should be noted that $H_p$ reveals a similar kind of variation over all three stations, suggesting that the pre-reversal vertical drift and the bottomside density gradient, are probably, not very different over these three stations. It is probably the different off-equatorial dynamics over three stations, which directly impact the bubble evolution, that may be responsible for drastic different variation of plume peak height $H_{pk}$.

### 4.3 Longitudinal effect of ESF parameters and forecasting of the plume

Aforementioned findings in Sect. 4.2 suggest that for a given solar flux and chosen season of maximum occurrence, the ionospheric conditions for the plume evolution, are most favourable over SLZ and comparatively less favourable over CXI while over ROJ, conditions are of intermediate characteristics. In other words, for any equatorial location located between SLZ and CXI, the bubble evolution characteristics should be between two extremes. This windowing may assist us to forecast the ESF parameters (within a certain band of tolerance) for a given equatorial station located between SLZ and CXI. In particular, the plume parameter $T_p$ and $H_p$ should be of primary concern as they are related to the occurrence of plume. We may note from Fig. 4 that for a given solar-flux, the $T_p$ increases almost linearly from SLZ towards CXI. Thus, for a given low solar-flux period, for any longitude in between SLZ and ROJ, the $T_p$ should be in between 20:00–21:00 LT. Similarly for any longitude in between ROJ and CXI, the $T_p$ should be in between 21:00–23:00 LT. For high solar-flux, the corresponding time band of tolerance should be 20:00–20:45 LT and 20:45–22:30 LT respectively. Thus, for any longitude between SLZ-CXI, it may be possible to obtain the onset-time of plume with 1–2 h of band of tolerance. This estimation is solely based on $T_p$. If more information, such as $T_i$ and $\Delta T$ are used, the band of tolerance may be be further narrowed down. Therefore, the trend of ESF parameters, shown in Fig. 4a–c, are useful to understand the dynamics of bubble evolution and its possible

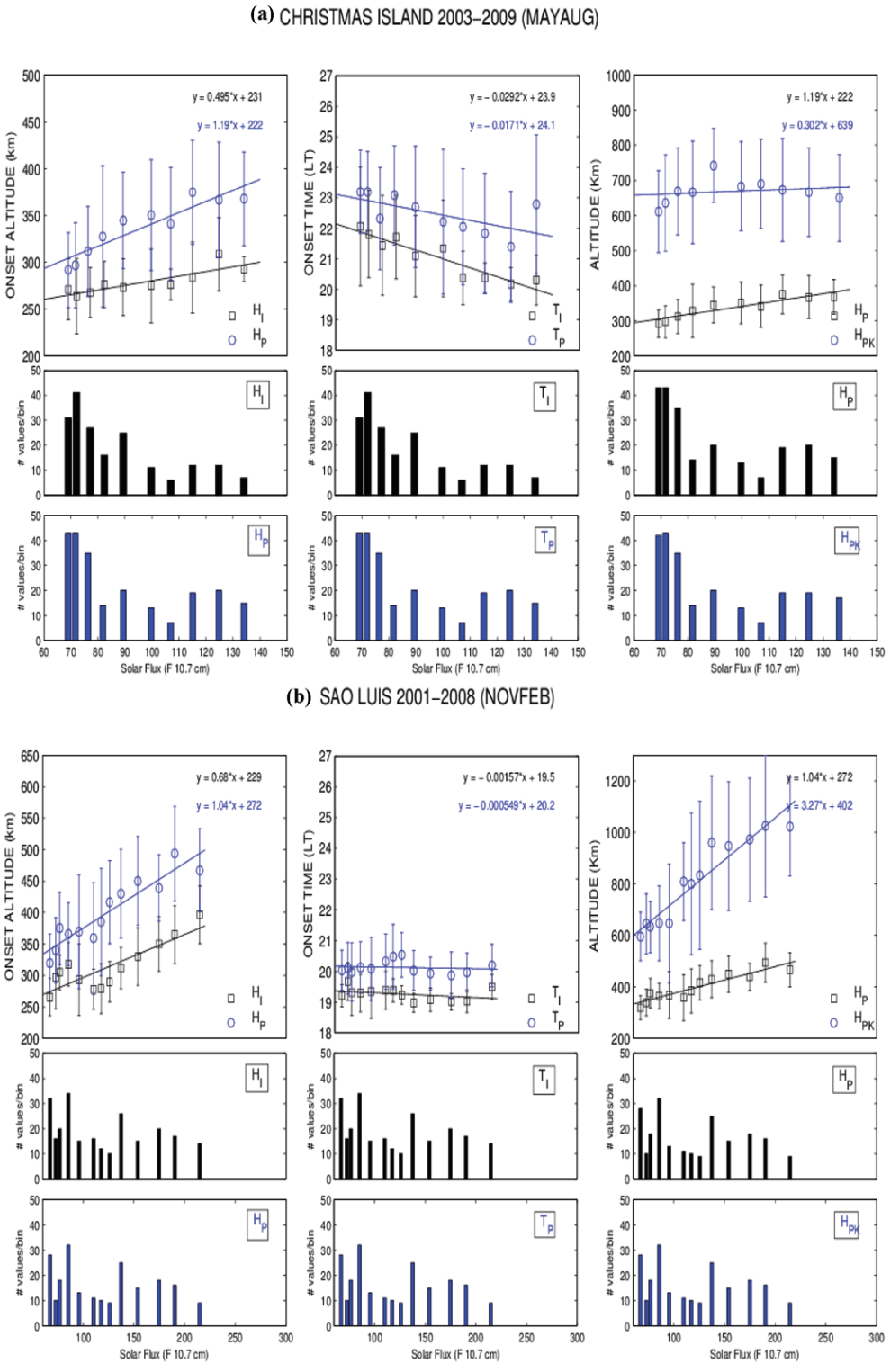


**Fig. 4.** VHF radar parameters for Christmas Island, São Luís and Jicamarca station, as a function of solar-flux. In the Fig. 4a–c, we depict the solar-flux dependence in the following format: in the upper panel from left-to-right columns, the ESF parameters ($H_i$, $H_p$), ($T_i$, $T_p$) and ($H_p$, $H_{pk}$) are plotted respectively. These values represent the 4 month average values and corresponding standard deviations are plotted as the error bars. In the middle-lower panels, the data-points that are used to estimate the average values in the corresponding upper panel, are shown.

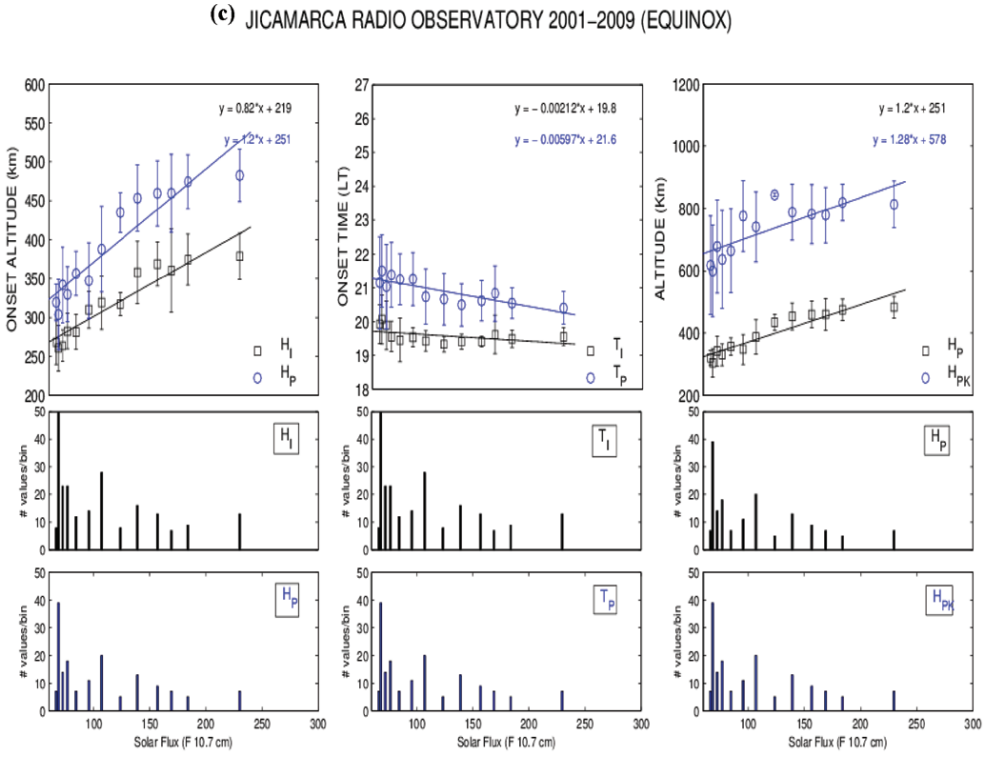


**Fig. 4.** Continued.

forecasting. For this purpose, in Fig. 4, we also provide the equations relating ESF parameters to the solar flux that are obtained using linear fitting. For any chosen ESF parameter, three equations from three longitudinally separated stations, provide a possibility to obtain the value of the parameter for any longitude located between SLZ and CXI. Such empirical relations for the ESF parameters allow to develop an empirical model which is important to study the evolution of irregularities in different longitudinal sectors, and for improving scintillation warning models. This empirical model is present in Table 4 covering seasons of maximum occurrence as well as the season of moderate occurrence. Each equation accompanies their respective R-square correlation number and standard deviation error of each coefficient in the linear correlation equation.

Figure 5 shows the occurrence of time parameters ($T_i$ in black and $T_p$ in white) as function of season and longitude, and irrespective of solar flux. Based on the methodology discussed above, the $T_p$ for any longitude in between SLZ and CXI can be estimated for any solar flux and season, using the characteristics shown in Fig. 5.

Figure 5 also reveals that the occurrence characteristics of ESF over CXI are very similar during equinox and summer-solstice, in contrast to the marked differences in these seasons over other two stations. It is known from previous studies that over CXI, the maximum ESF occurrence is during summer-solstice for low solar-flux and during equinox for high solar-flux. Since, the dataset for CXI used in the present study, covers mainly solar minimum, maximum occurrence during summer-solstice is noted in the present study. The very similar occurrence characteristics during equinox and summer-solstice, as noted in Fig. 5, suggests that, during solar maximum, the maximum ESF occurrence month may belong to equinox, as known from the previous studies.

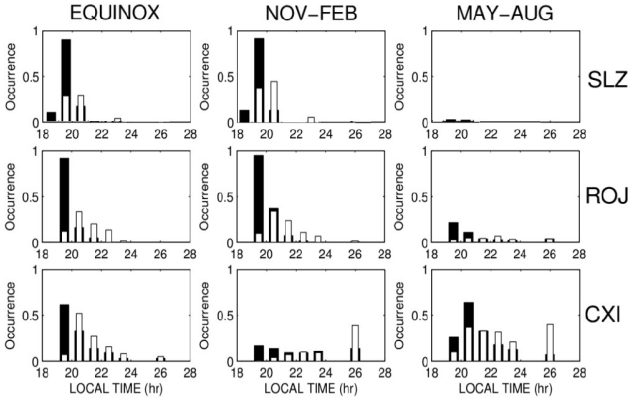


**Fig. 5.** Occurrence of $T_i$ (black bars) and $T_p$ (white bars) parameters as function of local time, showing seasonal variation, and irrespective of solar flux.

**Table 4.** VHF radar empirical model based on the linear relations of altitude and time parameters for São Luís, Jicamarca and Christmas Island equatorial stations.

| Season | Altitude parameter | Time parameter | |
|---|---|---|---|
| Equinox | $H_i$: $y = 0.577(\pm0.14)x + 241(\pm19.79)$; $R^2 = 0.64$<br>$H_p$: $y = 0.992(\pm0.29)x + 275(\pm42.07)$; $R^2 = 0.54$<br>$H_{pk}$: $y = 2.43(\pm0.51)x + 443(\pm73.30)$; $R^2 = 0.69$ | $T_i$: $y = -0.00351(\pm0.0008)x + 19.7(\pm0.12)$; $R^2 = 0.64$<br>$T_p$: $y = -0.00286(\pm0.0024)x + 20.4(\pm0.35)$; $R^2 = 0.20$ | São Luís |
| Nov–Feb | $H_i$: $y = 0.68(\pm0.13)x + 229(\pm16.73)$; $R^2 = 0.73$<br>$H_p$: $y = 1.04(\pm0.12)x + 272(\pm15.98)$; $R^2 = 0.87$<br>$H_{pk}$: $y = 3.27(\pm0.32)x + 402(\pm42.32)$; $R^2 = 0.91$ | $T_i$: $y = -0.00157(\pm0.0011)x + 19.5(\pm0.16)$; $R^2 = 0.20$<br>$T_p$: $y = -0.000549(\pm0.0012)x + 20.2(\pm0.17)$; $R^2 = 0.10$ | |
| Equinox | $H_i$: $y = 0.82(\pm0.09)x + 219(\pm11.56)$; $R^2 = 0.90$<br>$H_p$: $y = 1.2(\pm0.14)x + 251(\pm17.88)$; $R^2 = 0.87$<br>$H_{pk}$: $y = 1.28(\pm0.30)x + 578(\pm39.00)$; $R^2 = 0.63$ | $T_i$: $y = -0.00212(\pm0.001)x + 19.8(\pm0.15)$; $R^2 = 0.23$<br>$T_p$: $y = -0.00597(\pm0.001)x + 21.6(\pm0.16)$; $R^2 = 0.70$ | Jicamarca |
| Nov–Feb | $H_i$: $y = 0.823(\pm0.05)x + 211(\pm6.60)$; $R^2 = 0.96$<br>$H_p$: $y = 1.01(\pm0.11)x + 296(\pm15.43)$; $R^2 = 0.87$<br>$H_{pk}$: $y = 1.1(\pm0.23)x + 573(\pm31.59)$; $R^2 = 0.67$ | $T_i$: $y = -0.00201(\pm0.001)x + 20.1(\pm0.15)$; $R^2 = 0.23$<br>$T_p$: $y = -0.00364(\pm0.0019)x + 21.6(\pm0.28)$; $R^2 = 0.22$ | |
| Equinox | $H_i$: $y = 0.522(\pm0.16)x + 225(\pm15.71)$; $R^2 = 0.60$<br>$H_p$: $y = 1.03(\pm0.44)x + 239(\pm42.78)$; $R^2 = 0.44$<br>$H_{pk}$: $y = 1.07(\pm0.62)x + 576(\pm59.86)$; $R^2 = 0.30$ | $T_i$: $y = -0.0236(\pm0.007)x + 22.4(\pm0.68)$; $R^2 = 0.62$<br>$T_p$: $y = -0.0194(\pm0.006)x + 23.1(\pm0.58)$; $R^2 = 0.60$ | Christmas Island |
| Nov–Feb | $H_i$: $y = 0.599(\pm0.23)x + 207(\pm19.70)$; $R^2 = 0.53$<br>$H_p$: $y = 1.5(\pm1.001)x + 187(\pm82.85)$; $R^2 = 0.30$<br>$H_{pk}$: $y = 1.78(\pm1.05)x + 493(\pm89.09)$; $R^2 = 0.30$ | $T_i$: $y = -0.0323(\pm0.009)x + 24.7(\pm0.79)$; $R^2 = 0.67$<br>$T_p$: $y = -0.00429(\pm0.011)x + 24.4(\pm0.94)$; $R^2 = 0.10$ | |
| May–Aug | $H_i$: $y = 0.495(\pm0.11)x + 231(\pm10.98)$; $R^2 = 0.70$<br>$H_p$: $y = 1.19(\pm0.18)x + 222(\pm17.84)$; $R^2 = 0.85$<br>$H_{pk}$: $y = 0.302(\pm0.52)x + 639(\pm51.421)$; $R^2 = 0.10$ | $T_i$: $y = -0.0292(\pm0.004)x + 23.9(\pm0.39)$; $R^2 = 0.8$<br>$T_p$: $y = -0.0171(\pm0.007)x + 24.1(\pm0.72)$; $R^2 = 0.40$ | |

## 5 Conclusions

In the present work, we examine the seasonal, solar flux and longitudinal dependence of ESF occurrence, based on the observations from three equatorial stations: São Luís (SLZ), Jicamarca (ROJ) and Christmas Island (CXI). To do so, ESF is characterised by the following parameters: ($T_i$, $H_i$) representing the time and altitude of the first appearance of bottom-type/bottom-side irregular layers, ($T_p$, $H_p$, $H_{pk}$) representing the time and altitude of the first appearance of the plume, and the peak altitude of the plume respectively. While the seasonal and solar flux dependence characteristics of these parameters over SLZ and ROJ are known from the previous studies, the present study reveals new aspects of the

ESF occurrence over CXI and the variations of these parameters from three longitudinally separated equatorial stations.

The present study reveals the following seasonal characteristics: (1) the season of maximum % occurrence of ESF is summer-solstice (May–August for CXI and November–February for SLZ/ROJ) for all three stations, (2) % occurrence of the bottom-type ESF is seasonal dependent over SLZ/ROJ as compared to the no seasonal dependence over CXI, (3) total % occurrence of ESF, bottom-type ESF and plume during season of maximum occurrence is lowest over CXI and highest over SLZ, (4) over CXI, the ESF and plume occurrence are delayed by 2–3 h in comparison to SLZ/ROJ. These aspects suggest that the Ionospheric-Atmospheric conditions over SLZ (CXI) are most (least) favourable for the generation of ESF, among three stations. It is further interesting to note that the season of maximum occurrence of all ESF events (i.e. with and without plume) is summer-solstice for all three stations. Thus, as far as the generation of ESF is concerned, the summer-solstice season offers most favourable conditions.

Aforementioned seasonal difference in maximum occurrence over three stations is possibly, owing to the finite magnetic declination angle effect as explained by de Paula et al. (2011) based on the mechanism suggested by Abdu et al. (1981) for SLZ and ROJ. The declination effects in the occurrence of ESF with plume between SLZ and ROJ is reported by these studies. However, with the inclusion of CXI, the present study shows that the similar declination effects are present over CXI which has declination angle, intermediate of SLZ and ROJ. It is also noted that the occurrence of ESF with plume, and not the total ESF occurrence, that is controlled by the declination angle.

The solar flux dependence characteristics reveal that over CXI, the ESF parameters have similar solar-flux dependency as observed over other two stations. However, in contrast to other two stations, over CXI, with increasing solar-flux, the plume appearance is delayed and the vertical extent of the plume become shorter. These characteristics suggest that over CXI, the plume occurrences are more favourable during low solar-flux.

It may be mentioned that the gravity wave activity, which act as a seeding perturbation, may be very different for solar-minimum/maximum and over these three stations and these differences may also account for different ESF/plume behaviour over these three stations.

The present comparative study over three equatorial stations suggests that for a given solar-flux and chosen season of maximum occurrence, the ionospheric conditions for the plume evolution, are most favourable over SLZ and comparatively less favourable over CXI while over ROJ, conditions are of intermediate characteristics. In other words, for any equatorial location located between SLZ and CXI, the bubble evolution characteristics should be between two extremes. This windowing may assist to forecast the ESF parameters (within certain band of tolerance) for a given equatorial station located between SLZ and CXI which is important to study the evolution of irregularities in different longitudinal sectors, for improving scintillation warning models.

*Acknowledgements.* We thanks FAPESP under projects 2008/00138-4 and 2012/25396-1 for supporting this research. We are very thankful to Jicamarca, São Luís and Christmas Island researchers and technical teams for providing the historical radar data needed for this study. The early Christmas Island radar data were collected by Roland Tsunoda with funds from National Science Foundation, ATM-0001678. More recent data were collected by Keith Groves with funds from AFRL. The authors are very thankful to Bela Fejer for his advices on this paper. E. R. de Paula is grateful for the partial support from AFOSR FA9550-10-1-0564 and CNPq 305684/2010-8 grants.

Topical Editor L. Blomberg thanks D. Chakrabarty and two anonymous referees for their help in evaluating this paper.

## References

Abdu, M. A.: Outstanding problems in the equatorial ionosphere-thermosphere electrodynamics relevant to spread F, J. Atmos. Sol.-Terr. Phys., 63, 869–884, 2001.

Abdu, M. A.: Equatorial ionosphere-thermosphere system: Electrodynamics and Irregularities, Adv. Space Res., 35, 771–787, 2005.

Abdu, M. A., Bittencourt, J. A., and Batista, I. S.: Magnetic declination control of the equatorial F region dynamo electric field development and Spread F, J. Geophys. Res., 86, 11443–11446, 1981.

Abdu, M. A., Medeiros, R. T., Bittencourt, J. A., and Batista, I. S.: Vertical ionization drift velocities and range type spread F in the evening equatorial ionosphere, J. Geophys. Res., 88, 399–402, 1983.

Basu, S., Basu, S., Aarons, J., McClure, J. P., and Cousins, M. D.: On the coexistence of kilometer-and meter-scale irregularities in the nighttime equatorial F region, J. Geophys. Res., 83, 4219–4226, 1978.

Basu, S., Basu, S., Mullen, J. P., and Bushby, A.: Long-term 1.5 GHz amplitude scintillation measurements at the magnetic equator, Geophys. Res. Lett., 7, 259–262, doi:10.1029/GL007i004p00259, 1980.

Chapagain, N. P., Fejer, B. G., and Chau, J. L.: Climatology of post-tunset equatorial spread F over Jicamarca, J. Geophys. Res., 114, A07307, doi:10.1029/2008JA013911, 2009.

de Paula, E. R. and Hysell, D. L.: The São Luís 30 MHz coherent scatter ionospheric radar: system description and initial results, Radio Sci., 39, RS1014, doi:10.1029/2003RS002914, 2004.

de Paula, E. R., Iyer, K. N., Hysell, D. L., Rodrigues, F. S., Kherani, E. A., Jardim, A. C., Rezende, L. F. C., Dutra, S. G., and Trivedi, N. B.: Multi-technique investigations of storm-time ionospheric irregularities over the São Luís equatorial station in Brazil, Ann. Geophys., 22, 3513–3522, doi:10.5194/angeo-22-3513-2004, 2004.

de Paula, E. R., Alam Kherani, E., Cueva, R. Y. C., and Camargo, L. A. P.: Observations of pre-midnight 5-m irregularities in the equatorial F region over São Luís. Brazil: solar-flux dependence

and seasonal variations, J. Atmos. Sol.-Terr. Phys., 73, 11–12, doi:10.1016/j.jastp.2011.03.014, 2011.

Farley, D. T., Basley, B. B., Woodman, R. F., and McClure, J. P.: Equatorial spread F: Implications of VHF radar observations, J. Geophys. Res., 75, 7199–7216, 1970.

Farley, D. T., Bonelli, E., Fejer, B. G., and Larsen, M. F.: The prereversal enhancement of the zonal electric field in the equatorial ionosphere, J. Geophys. Res., 91, 13723–13728, 1986.

Fejer, B. G., Scherliess, L., and de Paula, E. R.: Effect of the vertical plasma drift velocity on the generation and evolution of equatorial spread F, J. Geophys. Res., 104, 19859–19869, 1999.

Haerendel, G., Eccles, J. C., and Çakir, S.: Theory for Modeling the equatorial evening ionosphere and the origin of the shear in the horizontal plasma flow, J. Geophys. Res., 97, 1209–1223, 1992.

Hysell, D. L.: A review and synthesis of plasma irregularities in equatorial spread F, J. Atmos. Sol.-Terr. Phys., 62, 1037–1056, 2000.

Hysell, D. L. and Burcham, J.: JULIA radar studies of equatorial spread F, J. Geophys. Res., 103, 29155–29167, 1998.

Hysell, D. L. and Burcham, J.: Long term studies of equatorial spread F using the JULIA radar at Jicamarca, J. Atmos. Terr. Phys., 64, 1531–1543, 2002.

Hysell, D. L. and Farley, D. T.: Implications of the small aspect angles of equatorial spread F, J. Geophys. Res., 101, 5165–5176, 1996.

Jayachandran, B., Ballan, N., Rao, P. B., Sastri, J. H., and Bailey, G. J.: HF Doppler and ionosonde observations on the onset conditions of equatorial spread F, J. Geophys. Res., 98, 13741–13750, 1993.

Kudeki, E. and Bhattacharyya, S.: Postsunset vortex in equatorial F-region plasma drifts and implications for bottomside spread-F, J. Geophys. Res., 104, 28163–28170, 1999.

Kudeki, E., Akgiray, A., Milla, M., Chau, J. L., and Hysell, D. L.: Equatorial spread F initiation: Post-sunset vortex, thermospheric winds, gravity waves, J. Atmos. Sol.-Terr. Phys., 69, 2416–2427, 2007.

Makela, J. J., Ledvina, B. M., Kelley, M. C., and Kintner, P. M.: Analysis of the seasonal variations of equatorial plasma bubble occurrence observed from Haleakala, Hawaii, Ann. Geophys., 22, 3109–3121, doi:10.5194/angeo-22-3109-2004, 2004.

Makela, J. J., Kelley, M. C., and Tsunoda, R. T.: Observations of midlatitude ionospheric instabilities generating meter-scale waves at the magnetic equator, J. Geophys. Res., 114, A01307, doi:10.1029/2007JA012946, 2009.

Miller, E. S., Makela, J. J., and Kelley, M. C.: Seeding of equatorial plasma depletions by polarization electric fields from middle latitudes: Experimental evidence, Geophys. Res. Lett., 36, L18105, doi:10.1029/2009GL039695, 2009.

Miller, E. S., Makela, J. J., Groves, K. M., Kelley, M. C., and Tsunoda, R. T.: Coordinated study of coherent radar backscatter and optical airglow depletions in the central Pacific, J. Geophys. Res., 115, A06307, doi:10.1029/2009JA014946, 2010.

Ossakow, S. L.: Spread-F theories – A review, J. Atmos. Terr. Phys., 43, 437–452, 1981.

Rishbeth, H.: Polarization fields produced by winds in the equatorial F region, Planet. Space., 19, 357–369, 1971.

Rodrigues, F. S., de Paula, E. R., Abdu, M. A., Jardim, A. C., Iyer, K. N., Kintner, P. M., and Hysell, D. L.: Equatorial spread F irregularity characteristics over São Luís, Brazil, Radio Sci., 39, RS1S31, doi:10.1029/2002RS002826, 2004.

Rodrigues, F. S., Hysell, D. L., and de Paula, E. R.: Coherent backscatter radar imaging in Brazil: large-scale waves in the bottomside F-region at the onset of equatorial spread F, Ann. Geophys., 26, 3355–3364, doi:10.5194/angeo-26-3355-2008, 2008.

Sobral, J. H. A., Abdu, M. A., Takahashi, H., Taylor, M. J., de Paula, E. R., Zamlutti, C. J., de Aquino, M. G., and Borba, G. L.: Ionospheric plasma bubble climatology over Brazil based on 22-years (1977–1998) of 630 nm airglow observations, J. Atmos. Sol.-Terr. Phys., 64, 1517–1524, 2002.

Tsunoda, R. T.: On the spatial relationship of 1-m equatorial spread F irregularities and plasma bubbles, J. Geophys. Res., 85, 185–190, 1980a.

Tsunoda, R. T.: Magnetic-field-aligned characteristics of plasma bubbles in the equatorial ionosphere, J. Atmos. Terr. Phys., 42, 743–752, 1980b.

Tsunoda, R. T., Baron, M. J., Owen, J., and Towle, D. M.: ALTAIR, An incoherent scatter radar for equatorial spread F studies, Radio Sci., 14, 1111–1119, 1979.

Tsunoda, R. T., Livingston, R. C., Buonocore, J. J., and McKinley, A. V.: The frequency-agile radar: A multifunctional approach to remote sensing of the ionosphere, Radio Sci., 30, 1623–1643, 1995.

Woodman, R. F. and Hagfors, T.: Methods for the measurement of Vertical Ionospheric Motions near the Magnetic Equator by Incoherent Scattering, J. Geophys. Res., 74, 1205–1212, 1969.

Woodman, R. F. and La Hoz, C.: Radar observations of F region equatorial irregularities, J. Geophys. Res., 81, 5447–5466, 1976.